ELSEVIER

Nuclear Instruments and Methods in Physics Research B 135 (1998) 16–24

NIM B
Beam Interactions with Materials & Atoms

Atomic processes of high energy heavy ions channeled in a crystal

K. Komaki [1]

Institute of Physics, Graduate School of Arts and Sciences, University of Tokyo, Komaba, Meguro, Tokyo 153, Japan

Abstract

Swift heavy ions channeled in a crystal experience a variety of atomic processes which depend on the ion trajectory in the channel. Recent studies on the atomic processes such as slowing down of the ion, charge changing collision, excitation of bound electrons, and so on in connection with ion trajectories or impact parameter are reviewed. Resonant coherent excitation (RCE) is a composition of various atomic processes and has offered a new field in atomic physics and has been investigated experimentally and theoretically. Recent progress in this field is also reviewed. © 1998 Elsevier Science B.V.

PACS: 61.85; 34.50; 34.70
Keywords: Channeling; Heavy ion; Relativistic energy; Resonant coherent excitation; Charge state; Stopping power; Trajectory dependence

1. Introduction

Since the early period of channeling experiments, transmission measurements have been performed as well as backscattering measurements [1]. In the backscattering experiment, main objectives of the measurement are signals from close encounter processes. On the other hand, it has been noticed that swift channeled ions are subject to a variety of atomic collision processes. Transmission measurements, where the final states of the ions are detected, are suitable methods to obtain information on these atomic processes experienced by the channeled ion.

Trajectories of channeled ions are confined in a region far from atomic strings or planes and their collision partners are restricted mainly to valence electrons. This situation gives rise to a special collision system of an energetic ion and a dense electron target. The crystal furthermore provides a peculiar environment to the traveling ion. The continuum potential not only governs the ion trajectory but also acts on the bound electrons as a strong electrostatic field as high as $\sim 10^{10}$ V/m. A dynamic response of valence electrons, the wake, exerts a stationary backward electric field on bound electrons as well as on the whole ion. The latter effect is observed as the stopping power. The effects of the continuum and wake potentials on the bound electrons result in Stark shifts of the energy levels and Stark mixing of otherwise degenerated subshell levels. While the former effect is

[1] E-mail: komaki@phys.c.u-tokyo.ac.jp.

PII S0168-583X(97)00640-X

in the transverse direction, the latter is in the longitudinal direction. This situation may bring about alignment of the bound electrons.

The discreteness of the crystal lattice along the ion trajectory plays interesting roles in some cases. A bound electron to the ion can react to this oscillatory field, which is the resonant coherent excitation (RCE).

The energy loss of a channeled ion is known to be substantially reduced reflecting the electron density probed by the ion. Probabilities of the electron loss and capture processes of channeled ions also depend on the electron density encountered by the ion. Besides, the relative velocity between the ion and the electron plays an important role in charge changing collisions. Thus, these processes exhibit specific dependence on the position of the ion, i.e., the ion trajectory.

On the other hand, the exit direction of the ion is closely correlated with the ion trajectory in the crystal channel through the conservation rule of the transverse energy.

When some of these quantities are measured in coincidence, that is, signals originated from the same ion are obtained, correlation among these quantities provides information on the nature of these processes. In the following, recent researches on the atomic processes in connection with ion trajectories or impact parameter are reviewed.

Among other subjects, RCE will be described in detail because it provides a field for experimental and theoretical studies on various atomic processes experienced by heavy ions traveling in a crystal channel.

2. Experimental techniques

Recent development in high energy accelerators and highly charged heavy ion sources, such as electron cyclotron resonance ion source, made a vast variety of ion species available for channeling measurement. For channeling experiments, a beam of mono-energetic beam has to be collimated within an order of the critical angles:

$$\psi_1 = \sqrt{4Z_1Z_2e^2/pvd}, \tag{1}$$

$$\psi_p = \sqrt{4\pi Z_1Z_2e^2Na_{TF}d_p/pv}, \tag{2}$$

where Z_1 and Z_2 are the atomic numbers of the projectile ion and target atom, $p = \gamma M_1 v$ and v the momentum and velocity of the projectile, d the atomic spacing along the channeling axis and Nd_p is the areal density of atoms in the channeling plane.

The incident energy, charge state and direction of the ion relative to the crystal are fundamental parameters defining the experimental conditions. The crystal thickness, t, is another important parameter. One of the measures for the thickness is the period of trajectory oscillation, λ, which is of the order of d_p/ψ_p for planar case. Other measures for the thickness are mean free passes for charge changing collisions and a length required for a significant amount of energy loss.

Objectives of the measurement are charge state, energy and angle of the exit ion, energies and directions of emitted photons and electrons and so on. To determine the exit angle, a detector with a defining aperture or a position sensitive detector (PSD) is used. Various types of two-dimensional (2D) PSD are also available.

The exit energy of the ion is usually measured by a solid state detector (SSD). When higher precision is needed, a magnetic spectrometer is used. If we use an SSD as a target, deposited energy to it can be measured with much higher precision than measuring energies of transmitted ions.

3. Exit angle and ion trajectory

For not too thick crystals, the exit angle of an ion with entrance position, $\boldsymbol{r}_{\perp in}$, and angle, $\boldsymbol{\psi}_{in}$, is represented by,

$$\boldsymbol{\psi}_{ex} = \boldsymbol{\psi}_{ex}(\boldsymbol{r}_{\perp in}, \boldsymbol{\psi}_{in};\ t) \tag{3}$$

and is a continuous function of the entry point $\boldsymbol{r}_{\perp in}$. In special cases such as $d\psi_{ex}/dx_{in} = 0$ for planar channeling or $\partial(\psi_{exx}, \psi_{exy})/\partial(x_{in}, y_{in}) = 0$ for axial channeling, the exit angle distribution forms a peak (rainbow effect). It should be noted that the distribution is determined by a universal parameter, the reduced thickness,

$$\tau = t/\lambda \propto t\sqrt{Z_1/pv}. \quad (4)$$

Krause et al. demonstrated that a Monte Carlo simulation successfully reproduces 2D distributions of exit angle of transmitted ions in the case where 20-MeV C^{6+} is impinged in the [0 0 1] direction of 1792 Å thick silicon crystal [2]. Comparison of observed 2D distributions for various reduced thickness, τ, which were realized by changing the beam energy, with simulated ones allows us to determine precise thickness of the crystal and to test adequacy of employed interaction potential.

In the planar case, the situation is greatly simplified, since the transverse motion is one dimensional and solvable. A segment of the oscillatory trajectory of the ion with the transverse energy, $E_\perp$, is given by

$$z = \zeta(x, E_\perp) \equiv \int_0^x \mathrm{d}x \, \sqrt{E/\{E_\perp - U(x)\}}, \quad (5)$$

where $U(x)$ is the planar continuum potential. The amplitude, $a(E_\perp)$, and the period, $\lambda(E_\perp)$, of the oscillation are given by

$$U(a(E_\perp)) \equiv E_\perp \text{ or } a(U(x)) \equiv x, \quad (6)$$

$$\lambda(E_\perp) = 4\zeta(a(E_\perp), E_\perp). \quad (7)$$

When an ion enters the crystal at the position, x_{in}, and with the incident angle, ψ_{in} and transmitted the crystal of thickness, t, at the exit position, x_{ex}, with the exit angle, ψ_{ex}, the following relations hold:

$$t = \frac{1}{2}n\lambda(E_\perp) + \left\{\frac{1}{4}\lambda(E_\perp) - \zeta(x_{in}, E_\perp)\right\}\mathrm{sgn}(\psi_{in}) - \left\{\frac{1}{4}\lambda(E_\perp) - \zeta(x_{ex}, E_\perp)\right\}\mathrm{sgn}(\psi_{ex}), \quad (8)$$

$$E_\perp = E\psi_{in}^2 + U(x_{in}) = E\psi_{ex}^2 + U(x_{ex}), \quad (9)$$

where $\mathrm{sgn}(x)$ is the sign function, n is an integer representing the number of times the ion is bounced by the atomic planes. If ψ_{in} and ψ_{ex} have the same sign, n is an even number and if ψ_{in} and ψ_{ex} have opposite signs, n is an odd number. For a given set of ψ_{in}, ψ_{ex} and t, possible ion trajectories are restricted, in general, to several cases indexed by n, each of which corresponds to different values of $E_\perp$ and thus to $\lambda(E_\perp)$ and $a(E_\perp)$.

Fig. 1 shows a 2D mapping of ψ_{ex} distribution, $Y(q_{ex}, \psi_{ex}; \psi_{in}, q_{in}, t)$, of 100 MeV O-ions transmitted through a Si crystal with $t = 0.95$ μm, as a function of the entrance angle, ψ_{in}, with respect to the (2 2 0) plane, in the case where incident and exit charge states are $q_{ex} = q_{in} = 8$ [3]. The total yield for each incident angle is normalized. In this 2D display, several characteristic features are noticed. When incident angle satisfies the channeling condition (critical angle is ~1.3 mrad for bare ions), several peaks appear along the lines of $\psi_{in} = \pm\psi_{ex}$. These peaks are formed by trajectories which satisfies the conditions $x_{in} = x_{ex} = 0$ and $t = \frac{1}{2}n\lambda$. Peaks on $\psi_{in} = \psi_{ex}$ and $\psi_{in} = -\psi_{ex}$ correspond to even and odd values of n, respectively, and they appear on each line alternatively.

Intensity distribution in the area around $\psi_{in} = \psi_{ex} = 0$ shows a sharp dependence on the thickness, which was used to determine crystal thickness by comparing with the simulation. In the planar case, the reduced thickness, $\tau = t/\lambda$, can be changed either by rotating the crystal keeping the channeling plane unchanged or by altering the beam energy.

A pair of valleys along the line of $\psi_{ex} = 0$ is due to the blocking effect. Finally, a broad ridge along

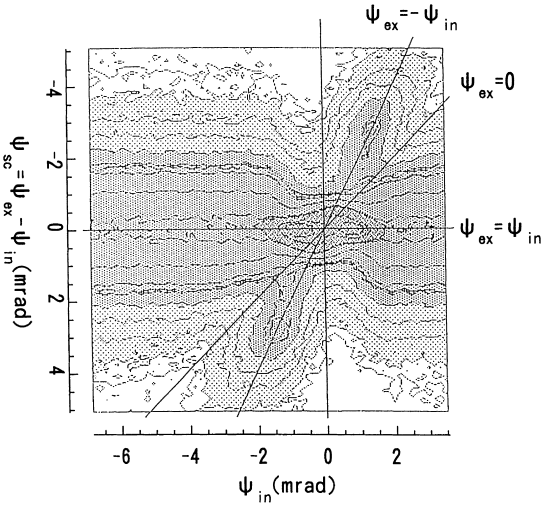

Fig. 1. A contour map of scattering angle distribution of 100 MeV O^{8+} ions transmitted through 0.95 μm thick Si crystal as a function of incident angle relative to the (2 2 0) plane.

the line of $\psi_{in} = \psi_{ex}$ outside the channeling condition is due to multiple scatterings.

4. Energy loss of the projectile

In view of the momentum transfer, the energy loss of the ion is divided into two parts contributed by close and distant collisions with target electrons. The fact that the energy loss of the channeled ion is roughly a half of random case has been well known and is understood as a reduction of the contribution from close collisions. To be more precisely, the stopping power for channeled ion depends on the ion position as $S(E,x)$. In the case of planar channeling in a relatively thick crystal, the position dependent stopping power, $S(E,x(z))$, can be averaged over the trajectory oscillation,

$$S(E,E_\perp) = (4/\lambda(E_\perp)) \int_0^{a(E_\perp)} S(E,x)\,\mathrm{d}x\,\sqrt{E/\{E_\perp - U(x)\}}. \tag{10}$$

Fig. 2 shows a contour map of energy deposition and exit angle distribution, $Y(\Delta E, \psi_{ex}; \psi_{in}, t)$, for 30 MeV C^{6+} ions transmitted through 4 μm thick Si in the case of $\psi_{in} = -1.57$ mrad. In this measurement, a totally depleted Si detector was used as the target and transmitted ions were detected, in coincidence, with a 2D-PSD placed downstream [4]. In the figure several peaks appear alternately on both sides of $\psi_{ex} = 0$ axis. Peaks on $\psi_{ex} > 0$ and $\psi_{ex} < 0$ sides are formed by ions bounced in the channel odd and even numbers of times, respectively. In their pioneering study of relation between energy loss, ΔE, and the number of oscillations or oscillation period, λ, Oak Ridge group deduced a position dependent stopping power, $S(E,x)$ [5,6].

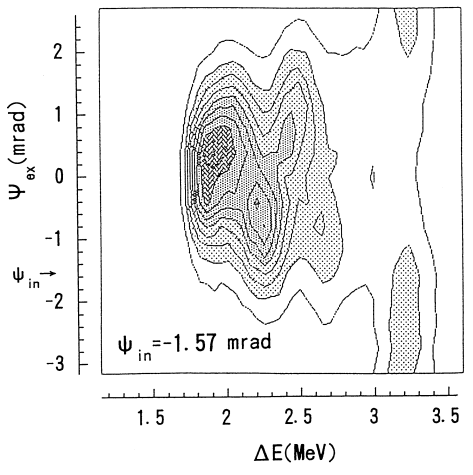

Fig. 2. A contour map of energy deposition and exit angle distribution for 30 MeV C^{6+} ions transmitted through 4 μm thick Si with incident angle −1.57 mrad with respect to (2 2 0) plane.

5. Exit charge state

Charge state of swift ions penetrating a solid target, in a random direction, quickly reaches an equilibrium distribution regardless of their initial charge state. For a channeled ion, the partners of the charge changing collisions are crystal electrons it encounters and both probabilities of electron capture and loss processes are reduced. Thus the ions tend to keep their initial charge states, which is called the frozen charge state.

An important parameter to govern the charge changing collision is the equivalent electron energy, $E_e = Em/M_1$, where m/M_1 is the electron to ion mass ratio. When E_e is below the binding energy, B_p, of the projectile electrons, the cross section for the electron impact ionization is small. As E_e increases, the cross section reaches its maximum at $E_e \sim B_p$ and then decreases. When E_e exceeds the binding energy, B_t, of the target electron, the capture cross section for that electron decreases rapidly.

In the channel center, electron density is substantially lower than the average and the deeply bound electrons with high velocities enough to be captured are much more rare. Accordingly, the probabilities of electron loss and capture for the channeled ion exhibit different dependence on the ion position.

Fig. 3 shows the yield, $Y(q_{ex}; \psi_{in}, q_{in}, t)$ for $q_{in} = 35$ and $q_{ex} = 37$ as a function of incident angle, ψ_{in}, for 27 MeV/u Xe ions channeled in [1 1 0] axis of silicon [7]. Much narrower width

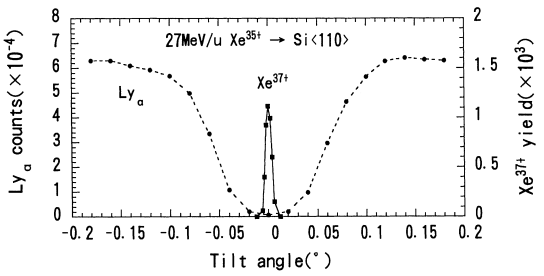

Fig. 3. Incident angle dependence of $q_{ex} = 37$ fraction and Lyman α intensity for 27 MeV/u Xe ($q_{in} = 35$) ions channeled in the [1 1 0] axis of silicon.

of the peak in comparison to a wide dip of Lyman α yield demonstrates that only hyperchanneled ions can retain such a low charge state.

Fig. 4 shows contour maps of charge state fractions, $Y(\psi_{ex}, q_{ex}; \psi_{in}, q_{in}, t)/\sum_{q_{ex}} Y(\psi_{ex}, q_{ex}; \psi_{in}, q_{in}, t)$, as functions of ψ_{in} and ψ_{ex} with $q_{in} = 6, 7$ and 8 and $q_{ex} = 6$ and 7 for 100 MeV O-ions transmitted through 0.95 μm silicon crystal [3]. The abscissa and ordinate of each map are the same as in Fig. 1. While nonchanneled ions achieved charge state equilibrium, charge state distribution around $\psi_{ex} \sim \psi_{in} \sim 0$, which corresponds to trajectories with small amplitudes, shows distinct charge state dependence. No intensity for $q_{ex} < q_{in}$ cases clearly demonstrates that ions transmitted along the channel center never capture electrons.

6. Resonant coherent excitation

Since the first observation of RCE of hydrogen-like heavy ions [8], RCE has been studied experimentally and theoretically in relation to various atomic processes [9].

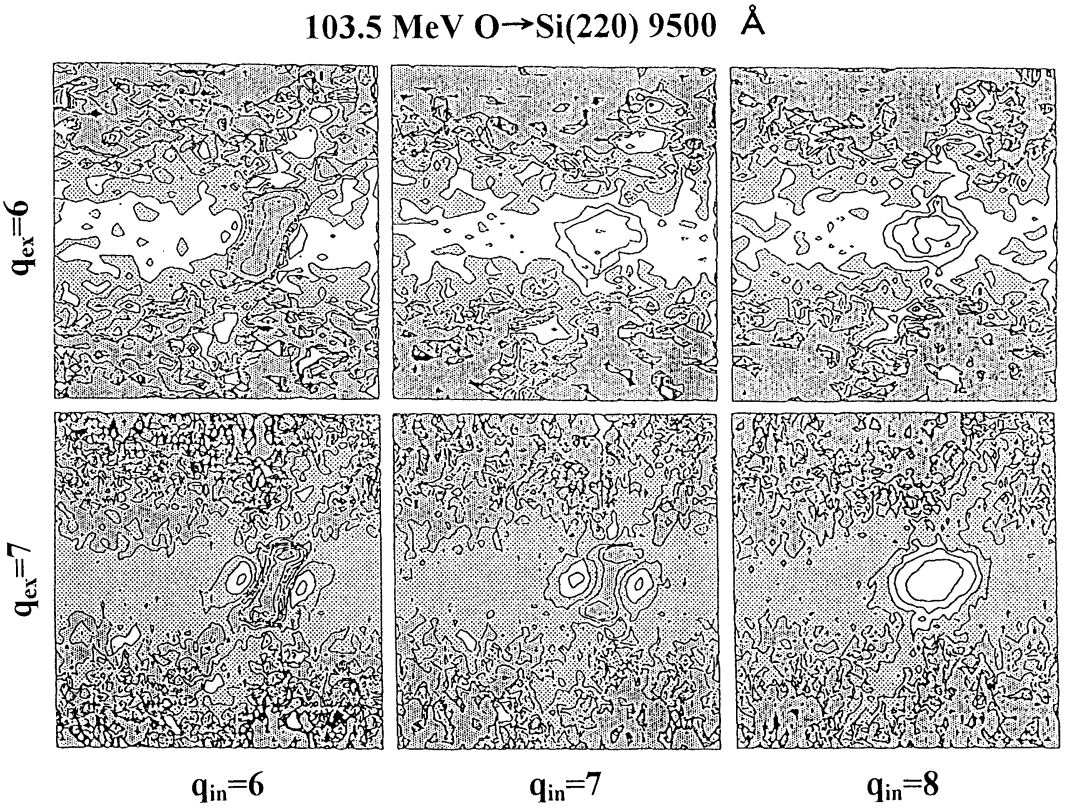

Fig. 4. Contour maps of fractions with exit charge states of 6 and 7, as functions of incident and exit angles for 100 MeV O transmitted through 0.95 μm silicon crystal with initial charge states of 6, 7 and 8.

6.1. Resonance conditions

The periodic electrostatic potential of the crystal can be expanded into a Fourier series,

$$\boldsymbol{\phi}(r) = \sum_{\boldsymbol{g}} \boldsymbol{\phi}_{\boldsymbol{g}} \exp(2\pi i \boldsymbol{g} \cdot \boldsymbol{r}), \tag{11}$$

where $\boldsymbol{g}$ is a reciprocal lattice vector. When an ion travels in a crystal with a constant velocity, $\boldsymbol{v}$, the trajectory of the ion is given by $\boldsymbol{R}(t) = \boldsymbol{R}_{\perp} + \boldsymbol{v}t$ and the potential seen by an electron bound to it,

$$\boldsymbol{\phi}(\boldsymbol{R} + \boldsymbol{r}) = \sum_{\boldsymbol{g}} \boldsymbol{\phi}_{\boldsymbol{g}} \exp(2\pi i \boldsymbol{g} \cdot \boldsymbol{v}t) \times \exp(2\pi i \boldsymbol{g} \cdot \boldsymbol{R}_{\perp}) \exp(2\pi i \boldsymbol{g} \cdot \boldsymbol{r}) \tag{12}$$

is a superposition of time-dependent fields with frequencies, $v = \boldsymbol{g} \cdot \boldsymbol{v}$. Here $\boldsymbol{r}$ is the position vector of the electron relative to the ion nucleus.

When the ion is axially channeled along a lattice vector $\boldsymbol{H}$, the velocity vector is given by $\boldsymbol{v} = \mathbf{H}v/d$, where $d = |\boldsymbol{H}|$ is the atomic spacing along the axis. In this case, those Fourier components $\boldsymbol{\phi}_{\boldsymbol{G}}$ which satisfy $\boldsymbol{G} \cdot \boldsymbol{H} = k =$ integer coherently contribute to a frequency $v(k) = \boldsymbol{G} \cdot \boldsymbol{v} = kv/d$. The RCE condition is then represented by the familiar formula,

$$\Delta E = hv(k) = h\boldsymbol{G} \cdot \boldsymbol{v} = khv/d. \tag{13}$$

When an ion travels parallel to an atomic plane, it feels the discreteness of the atomic plane as an array of atomic strings. In the same way as a set of atomic planes are represented by the Miller index (h_1, h_2, h_3), a set of atomic strings on a plane can be specified by a 2D Miller index, (k,l). Taking two lattice vectors, $\boldsymbol{H}_1$ and $\boldsymbol{H}_2$, as the base vector of 2D *crystal*, the closest string in the set to the coordinate origin intersects with two axes at $\boldsymbol{H}_1/k$ and $\boldsymbol{H}_2/l$. If the ion velocity, $\boldsymbol{v}$, makes angles θ and $\beta - \theta$ with $\boldsymbol{H}_1$ and $\boldsymbol{H}_2$, β being the angle between $\boldsymbol{H}_1$ and $\boldsymbol{H}_2$, the frequency for the ion to pass two adjacent strings is given by,

$$v(k,l) = (v/\sin\beta)[k\sin(\beta - \theta)/H_1 + l\sin\theta/H_2], \tag{14}$$

where $H_1 = |H_1|$ and $H_2 = |H_2|$ are atomic spacings along $\boldsymbol{H}_1$ and $\boldsymbol{H}_2$ axes. When $\boldsymbol{H}_1$ and $\boldsymbol{H}_2$ can be chosen perpendicular to each other, the resonance condition is given by,

$$\Delta E = hv(k,l) = hv[k\cos\theta/H_1 + l\sin\theta/H_2]. \tag{15}$$

6.2. Excitation amplitude

Taking z-axis parallel to the velocity, the field seen by the electron is rewritten as

$$\boldsymbol{\phi}(\boldsymbol{R} + \boldsymbol{r}) = \sum_{k} \boldsymbol{\phi}_k(X + x, Y + y, z) \exp(2\pi i v(k)t), \tag{16}$$

$$\boldsymbol{\phi}(\boldsymbol{R} + \boldsymbol{r}) = \sum_{kl} \boldsymbol{\phi}_{kl}(X + x, y, z) \exp(2\pi i v(k,l)t) \tag{17}$$

for axial and planar cases. Components with $k = 0$ and $k = l = 0$ are the continuum potential. Transition amplitude to the excited states are given by matrix elements of $\boldsymbol{\phi}_k(X + x, Y + y, z)$ or $\boldsymbol{\phi}_{kl}(X + x, y, z)$.

Reflecting specific symmetry of the crystal lattice, the excitation amplitude obeys an extinction rule just like in the case of diffraction phenomena. Krause et al. [10] observed that in the case of $\langle 1\ 1\ 1\rangle$ axial channeling of a diamond structured crystal, resonances for indices $k = 4n + 2$, n being an integer, are absent.

A similar example in the planar case is also reported [11]. Atomic configuration on a (2 $\bar{2}$ 0) plane in the diamond structure is shown in Fig. 5. 2D unit cell can be defined by two base vectors, $\boldsymbol{H}_1 = [1, 1, 0]a/2$ and $\boldsymbol{H}_2 = [0, 0, 1]a$, spacing along them being $H_1 = a/\sqrt{2}$ and $H_2 = a$. Since diamond structure has two atoms in a 2D cell, i.e., at the corner (0,0) and at (1/2,1/4), while the former atom always lies on any (k,l) string, the latter one lies $k/2 + l/4$ period off a string. Then the contribution from both atoms are completely destructive if $2k + l = 4n + 2$. Fig. 6 shows the survived fraction of 390 MeV/u Ar^{17+} channeled in (2 $\bar{2}$ 0) plane of Si crystal, as a function of tilt angle relative to the [1 1 0] axis. While resonances (1,1), (1,2), (1,3) are clearly seen as doublet and (1,5) and (1,6) are slightly recognized, the resonance (1,4) is not observed.

6.3. Stark effect

Stark field for an electron bound to the channeled ion consists of two components. One is the

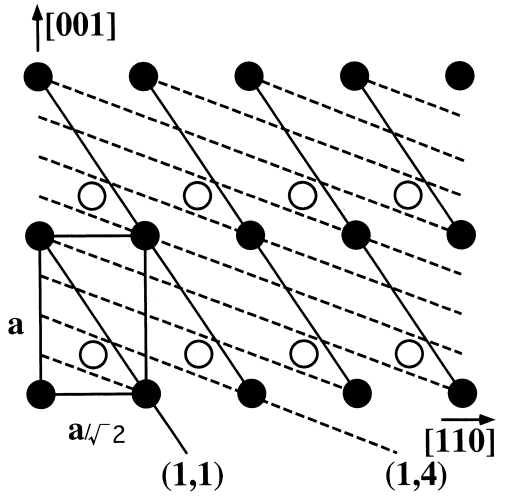

Fig. 5. Atomic arrangement on (2 $\bar{2}$ 0) plane of diamond structure. Solid lines indicate (1, 1) string and broken lines (1, 4) string.

static continuum potential and the other is the wake field which is induced by the ion and trails it, resulting in a stationary field on the electron. Magnitudes of these two contributions are comparable at relatively low (~10 MeV/u) energy region but in the relativistic energy region, the latter effect becomes negligibly small.

The wake field intermixes 2s and $2p_z$ state to form $2sp_z$(a) and $2sp_z$(b) states, of which electron clouds are centered ahead of and behind the ion, respectively, and $2p_x$ and $2p_y$ states remain nearly degenerated. Their energy eigen values are ordered as $E(2sp_z(b)) > E(2p_x) \sim E(2p_y) > E(2sp_z(a))$.

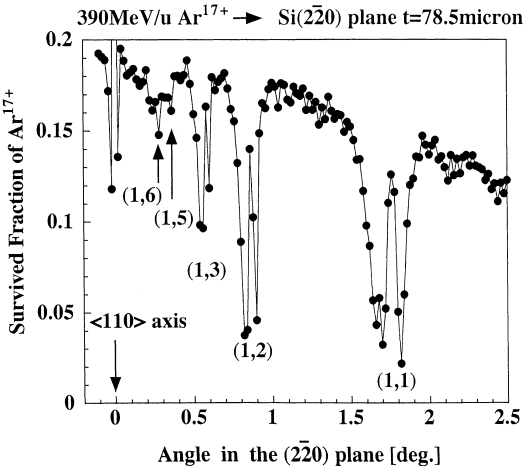

Fig. 6. Survived fraction of 390 MeV/u Ar^{17+} channeled in (2 $\bar{2}$ 0) plane of Si crystal, as a function of tilt angle relative to the [1 1 0] axis.

In the planar case, taking x-axis normal to the plane, the crystal field intermixes 2s and $2p_x$ states, resulting in $2sp_x$(c) and $2sp_x$(w) states with electron cloud extended toward the channel wall and toward the channel center, respectively. The split levels are arranged as $E(2sp_x(c)) > E(2p_y) \sim E(2p_z) > E(2sp_x(w))$. It should be noted that even at the channel center, where the electric field is absent, the curvature of the potential causes downward shift of energy levels reflecting the extent of electron cloud in x-direction.

In general, 2s, $2p_x$ and $2p_z$ are subject to mixing and resulting states changes their nature according to the ion position and relative strength of the two perturbations, and level crossing among them is avoided but $2p_y$ level remains pure and may cross former three levels.

In the case of axial channeling, the crystal field mixes 2s, $2p_x$ and $2p_y$ states and together with wake field forms more complex states.

For heavy ions where $\alpha Z_1 \sim Z_1/137$ is not small enough, LS coupling partially removes the degeneracy in vacuum states. Thus as unperturbed states, Dirac states have to be taken. Then the effect of the crystal and wake fields is qualitatively different from that in the lighter ion cases. Fig. 7 shows calculated shifts in the transition energy for $n=2$ sublevels for 390 MeV/u Ar^{+17} in Si (2 $\bar{2}$ 0) channel. In the figure two horizontal broken lines represent energy split between $j=3/2$ and 1/2 states in vacuum. It is to be noted that for a heavy ion like Ar^{17+}, this difference amounts to ~5 eV and is of a comparable magnitude with crystal field Stark splitting. In such a high energy case, the wake field plays little role.

6.4. Ion position dependence

Due to the position dependence of the oscillatory potential $\phi_k(X+x, Y+y, z)$ and $\phi_{kl}(X+x, y, z)$, excitation amplitudes for Stark mixed $n=2$ levels as well as the transition energies depend on ion position in the channel. Generally, the closer to the atomic string or wall, the larger the amplitude.

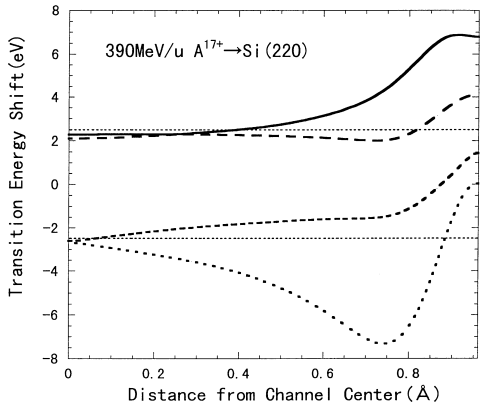

Fig. 7. Calculated shifts in the transition energy for $n=2$ sublevels for 390 MeV/u Ar^{17+} in Si (2 2 0) channel. Horizontal broken lines indicate unperturved transition energies to $j=3/2$ and 1/2 states.

For a planar channeled ion, the excitation amplitude is the largest at the maximum amplitude of the sinusoidal trajectory, where the ion position is stationary. Thus, the resonant excitation mostly takes place at maximum amplitudes.

Since the energy loss of the ion has a strong correlation with the amplitude of the trajectory, simultaneous measurements of the transition energy and the energy loss of excited ions give us information on the position dependent level energies. Forster et al. [12] simultaneously measured charge state and energy loss of transmitted ions in the case of fifth order resonance of Si^{13+} in Si $\langle 1\ 1\ 2\rangle$ axis. Resonance curve for high energy loss ions shows stronger and split resonance in comparison with low loss ions.

Azuma et al. [11] measured correlation between exit charge state and energy deposition in the target for 390 MeV/u Ar^{17+} channeled in (2 $\bar{2}$ 0) plane of Si and demonstrated that the relation between resonance angles and energy deposition for Stark split states are well explained by calculation based on unperturbed Dirac solution.

6.5. X-ray emission

In the original prediction of RCE by Okorokov [13], detection of deexcitation photon was suggested. Attempts to measure light emission from excited ions, however, were unsuccessful and high probability of electron impact ionization of excited electrons is considered as the reason. First detection of radiative decay was made by using heavier projectile, Ne^{9+}, where the orbital radius of the excited electron is still smaller than channel size [14].

More detailed study in photon emission was carried out for 160 MeV Mg^{11+} in Au$\langle 1\ 1\ 1\rangle$ axis [15]. Fig. 8 shows charge fraction of Mg^{12+} and Mg K-X-ray yield as function of beam energy. In both quantities, two resonance peaks are clearly seen. While X-ray intensity is almost same for two peaks, the high energy peak for 12+ fraction is much smaller than the low energy one, reflecting the fact that the low energy peak corresponds to transition to a $2p_x$–$2p_y$ dominant state and the high energy one to a $2p_z$-dominant state. The former has larger transverse size of electron cloud and has higher probability of subsequent electron impact ionization.

Datz et al. [16] measured, in addition to the exit charge state, X-rays in two directions, 45° and 90° for 25 MeV/u Mg^{11+} planar channeled in Ni (2 0 0) plane. In the charge state data, two resonances are observed. The wide, low energy one is attributed to $2sp_x$(w) state and sharp, middle energy one to nearly degenerated $2p_y$ and $2p_z$ states. $2sp_x$(c) state is observed as a shoulder in the high energy side. An enhancement in X-ray yield is observed with 90° detector at middle energy region, suggesting additional contribution from $2p_z$ state.

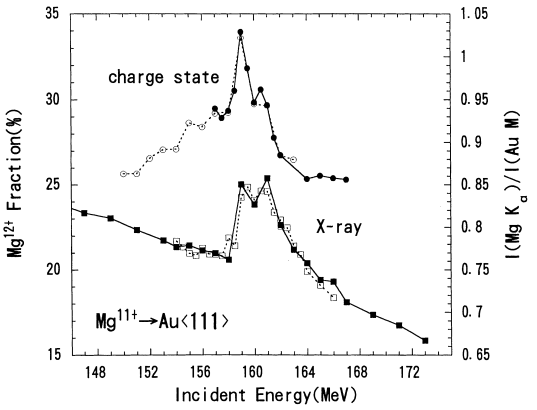

Fig. 8. Ionized fraction of Mg^{12+} and Mg K-X-ray yield as function of beam energy for Mg^{+11} incident on Au $\langle 1\ 1\ 1\rangle$ axis.

Through these investigations, it is now considered that atomic states inside the channel are heavily modified by the crystal and wake fields but electrons in these states are fairly well defined in spite of collisions with dense electrons in the channel.

References

[1] D.S. Gemmell, Rev. Mod. Phys. 46 (1974) 129.
[2] H.F. Krause, J.H. Barrett, S. Datz, P.F. Dittner, N.L. Jones, J. Gomez del Campo, C.R. Vane, Phys. Rev. A 49 (1994) 283.
[3] T. Azuma, K. Komaki, M. Yamagata, Y. Yamazaki, M. Sekiguchi, T. Hattori, T. Hasegawa, Nucl. Instr. and Meth. B 115 (1996) 310.
[4] T. Azuma, K. Komaki, Y. Yamazaki, N. Kakutani, S. Ninomiya, K. Maki, T. Takahira, M. Sekiguchi, T. Hattori, T. Hasegawa, Nucl. Instr. and Meth. B 115 (1996) 306.
[5] S. Datz, C.D. Moak, T.S. Noggle, B.R. Appleton, H.O. Lutz, Phys. Rev. 179 (1969) 315.
[6] M.T. Robinson, Phys. Rev. 179 (1969) 327.
[7] A. L'Hoir, S.A. Andriamonje, R. Anne, N.V. de Castro Faria, M. Chevallier, C. Cohen, J. Dural, M.J. Gaillard, R. Genre, M. Nage-Ali, R. Kirsch, B. Farizon-Mazuy, J. Mory, J. Moulin, J.C. Poizat, Y. Quéré, J. Remillieux, D. Schmaus, M. Toulemonde, Nucl. Instr. and Meth. B 48 (1990) 145.
[8] S. Datz, C.D. Moak, O.H. Crawford, H.F. Krause, P.F. Dittner, J. Gomez del Campo, J.A. Biggerstaff, P.D. Miller, P. Hvelplund, H. Knudsen, Phys. Rev. Lett. 40 (1978) 843.
[9] H.F. Krause, S. Datz, Channeling heavy ions through crystalline lattice, Adv. in Atomic, Molecular and Optical Physics 37 (1996) 139 and references therein.
[10] H.F. Krause, S. Datz, P.F. Dittner, N.L. Jones, C.R. Vane, Phys. Rev. Lett. 33 (1993) 348.
[11] T. Azuma, T. Ito, Y. Yamazaki, K. Komaki, M. Sano, M. Torikoshi, A. Kitagawa, E. Takada, T. Murakami, these Proceedings (ICACS-17), Nucl. Instr. and Meth. B 135 (1998) 61.
[12] J.S. Forster, G.C. Ball, W.G. Davies, J.S. Geiger, J.U. Andersen, J.A. Davies, H. Geissel, F. Nickel, Nucl. Instr. and Meth. B 107 (1996) 27.
[13] V.V. Okorokov, Yad. Fiz. 2 (1965) 1009 [Sov. J. Nucl. Phys. 2 (1966) 719].
[14] F. Fujimoto, K. Komaki, A. Ootuka, E. Vilalta, Y. Iwata, Y. Hirao, T. Hasegawa, M. Sekiguchi, A. Mizobuchi, T. Hattori, K. Kimura, Nucl. Instr. and Meth. B 33 (1988) 354.
[15] S. Datz, P.F. Dittner, J. Gomez del Campo, K. Kimura, H.F. Krause, T.M. Rosseel, C.R. Vane, Y. Iwata, K. Komaki, Y. Yamazaki, F. Fujimoto, Radiat. Eff. 117 (1991) 73.
[16] S. Datz, P.F. Dittner, H.F. Krause, C.R. Vane, O.H. Crawford, J.S. Forster, G.C. Ball, W.G. Davies, J.S. Geiger, Nucl. Instr. and Meth. B 100 (1995) 272.